Evidence of Water Vapor in Excess of Saturation in the Atmosphere of Mars

L. Maltagliati, *et al.*

Science **333**, 1868 (2011);
DOI: 10.1126/science.1207957

13. T. H. Zurbuchen *et al.*, *Science* **333**, 1862 (2011).
14. M. Hoshino, S. Zenitani, K. Nagata, Y. Takagi, in *Energy Budget in the High Energy Universe*, K. Sato, J. Hisano, Eds. (World Scientific, Singapore, 2007), pp. 108–118.
15. J. A. Slavin *et al.*, *Science* **329**, 665 (2010); 10.1126/science.1188067.
16. S. M. Krimigis, E. T. Sarris, in *Dynamics of the Magnetosphere*, S. I. Akasofu, Ed. (D. Reidel, Dordrecht, Netherlands, 1979), pp. 599–630.
17. E. T. Sarris, S. M. Krimigis, T. Iijima, C. O. Bostrom, T. P. Armstrong, *Geophys. Res. Lett.* **3**, 437 (1976).
18. S. P. Christon, J. Feynman, J. A. Slavin, in *Magnetotail Physics*, A. T. Y. Lui, Ed. (Johns Hopkins Univ. Press, Baltimore, MD, 1987), pp. 393–400.
19. D. N. Baker, J. E. Borovsky, J. O. Burns, G. R. Gisler, M. Zeilik, *J. Geophys. Res.* **92**, 4707 (1987).
20. G. L. Siscoe, N. F. Ness, C. M. Yeates, *J. Geophys. Res.* **80**, 4359 (1975).
21. G. C. Ho *et al.*, *Planet. Space Sci.*, 31 January 2011 (10.1016/j.pss.2011.01.011).

Acknowledgments: We thank the MESSENGER team for the development, cruise, orbit insertion, and Mercury orbital operations of the MESSENGER spacecraft. G.C.H. thanks M. Johnson, L. Brown, and J. Vandegriff for graphics support. The NASA Discovery Program under contract NAS5-97271 to The Johns Hopkins University Applied Physics Laboratory and contract NASW-00002 to the Carnegie Institution of Washington supports the MESSENGER mission to Mercury. MESSENGER data are available from NASA's Planetary Data System archive.

13 July 2011; accepted 5 September 2011
10.1126/science.1211141

Evidence of Water Vapor in Excess of Saturation in the Atmosphere of Mars

L. Maltagliati,[1]* F. Montmessin,[1] A. Fedorova,[2] O. Korablev,[2] F. Forget,[3] J.-L. Bertaux[1]

The vertical distribution of water vapor is key to the study of Mars' hydrological cycle. To date, it has been explored mainly through global climate models because of a lack of direct measurements. However, these models assume the absence of supersaturation in the atmosphere of Mars. Here, we report observations made using the SPICAM (Spectroscopy for the Investigation of the Characteristics of the Atmosphere of Mars) instrument onboard Mars Express that provide evidence of the frequent presence of water vapor in excess of saturation, by an amount far surpassing that encountered in Earth's atmosphere. This result contradicts the widespread assumption that atmospheric water on Mars cannot exist in a supersaturated state, directly affecting our long-term representation of water transport, accumulation, escape, and chemistry on a global scale.

The atmosphere of Mars holds 10,000 times less water vapor than that of Earth. If precipitated at the surface, the martian atmospheric water would form a layer only 10 μm thick on average. However, water vapor on Mars is a very dynamic trace gas and is one of the most variable atmospheric constituents. The characterization of the seasonal and latitudinal variations of water vapor is based on 40 years of dedicated observations of its integrated column abundance (*1*–*5*), whereas water vapor vertical distribution has been only sparsely observed up to now. The latter is nevertheless a unique indicator of those vertical transport processes that control the hydrological activity of the planet (*6*). The first direct observations, obtained with the Auguste spectrometer on the Russian Phobos-2 spacecraft, revealed a sharp decline around 25 km (the hygropause level) connecting two layers of nearly constant concentration (*7*). The decline was interpreted to be the result of the conversion of water vapor into ice because a discrete cloud layer was observed in the altitude range of the vapor depletion zone. However, the Auguste data set covers a narrow equatorial strip and encompasses less than a martian month. Because of the lack of subsequent comparable measurements, our understanding of the vertical structure of water on Mars has been built on indirect observations (*8*–*10*) and theoretical studies of the martian climate by using general circulation models (GCMs). Near the surface, the vertical distribution is expected to be dominated by surface-atmosphere interactions (convection and frost sublimation and deposition), whereas at altitudes above 10 km the role of water ice clouds, which are nearly ubiquitous on Mars, should become dominant (*11*, *12*).

Martian climate models commonly assume that water vapor supersaturation cannot exist in the atmosphere: Any amount of water exceeding the equilibrium vapor pressure is immediately converted into ice (*11*). This hypothesis requires the existence of a condensation mechanism that acts instantaneously and ubiquitously. For this reason, the partial pressure of water vapor above the hygropause is expected to fall rapidly toward negligible values, establishing the perception of a martian water vapor profile resembling a two-step function, with water vapor well-mixed below the hygropause and sharply declining above. However, detailed microphysical models reveal that interactions between airborne particles and water vapor can affect the vertical confinement of water below the condensation level and its possible presence at higher altitudes (*13*). When condensation nuclei (assumed to be dust aerosols on Mars) are too rare, condensation is impeded and is thus unable to maintain water vapor at saturation level, leaving substantial amounts of excess vapor. Lack of condensation occurs frequently in the Earth's upper troposphere, where supersaturation levels as high as 50% with respect to ice have been reported (*14*).

The water vapor profile data set presented here was extracted from the SPICAM (Spectroscopy for the Investigation of the Characteristics of the Atmosphere of Mars) solar occultation observations. The SPICAM instrument onboard

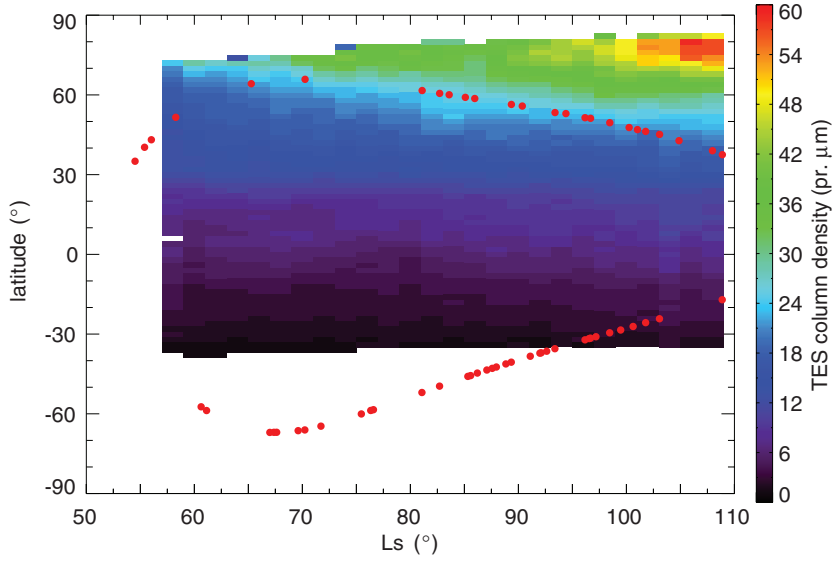

Fig. 1. SPICAM solar occultation positions shown by red dots as a function of L_s and latitude. TES water vapor column density retrievals (*19*) have been superimposed to indicate the corresponding activity of water vapor for the season during which the SPICAM measurements were taken.

[1]Laboratoire Atmosphères, Milieux, Observations Spatiales (LATMOS), 78280 Guyancourt, France. [2]Space Research Institute (IKI), 117997 Moscow, Russia. [3]Laboratoire de Météorologie Dynamique (LMD), 75252 Paris, France.

*To whom correspondence should be addressed. E-mail: luca.maltagliati@latmos.ipsl.fr

the European Space Agency (ESA) Mars Express spacecraft includes an infrared channel that probes the 1- to 1.7-μm spectral range with a resolution of 1 nm, allowing the identification and quantification of gaseous CO_2 and H_2O absorption features (*15*, *16*). Our inferred water vapor–mixing ratio profiles have a typical vertical resolution of 4 to 5 km and thus capture variations smaller than the average Mars atmospheric scale height (8 to 12 km). The complete data set of solar occultation includes 700 orbits that span more than three martian years (MY). However, water vapor could be retrieved only after the first martian year of observations, owing to pointing problems of the solar occultation port and to the subsequent series of tests needed to find the optimal mode of observation. The 61 profiles of the MY 29 campaign (*17*) discussed here provide a consistent view of the temporal and spatial trends of water during the aphelion season, between solar longitude (L_s) = 50° to 120° (Fig. 1) (*18*). This season exhibits the annual peak of activity of the martian water cycle: A maximum amount of water vapor is observed in the north owing to sublimation and further advection of water from the northern polar regions, where both seasonal and residual layers of frost reside, whereas the southern hemisphere remains depleted in water vapor for most of the season (*1*–*3*). The Thermal Emission Spectrometer (TES) onboard Mars Global Surveyor recorded an average of 25 precipitable micrometers in the north and almost no water vapor in the south during the same period (*19*).

The profiles we retrieved can be compared with the predictions from the martian GCM developed at the Laboratoire de Météorologie Dynamique (LMD) as provided by the Mars climate database (MCD; version 4.3) (*20*). Although both observations and model simulations consistently indicate a decrease in water with altitude, the MCD underestimates the quantities of water vapor between 20 and 50 km by factors exceeding 10 (Fig. 2). Predicted mixing ratios are smaller than 1 part per million by volume (ppmv), whereas SPICAM observed values as high as 20 ppmv. This discrepancy cannot be explained by a difference in vertical mixing alone, suggesting instead a difference in the degree of water vapor saturation. The aphelion season is the coldest on Mars (when Mars is farthest from the Sun), and the average hygropause level is expected to reach its annual low. Assuming that water vapor is confined below the hygropause, the saturation height should be ~15 km (*2*). Our observations of large quantities of water vapor above this altitude are therefore puzzling. The saturation ratio is obtained by dividing the observed water vapor partial pressure by the phase equilibrium pressure given by the Goff-Gratch equation (Fig. 2) (*21*).

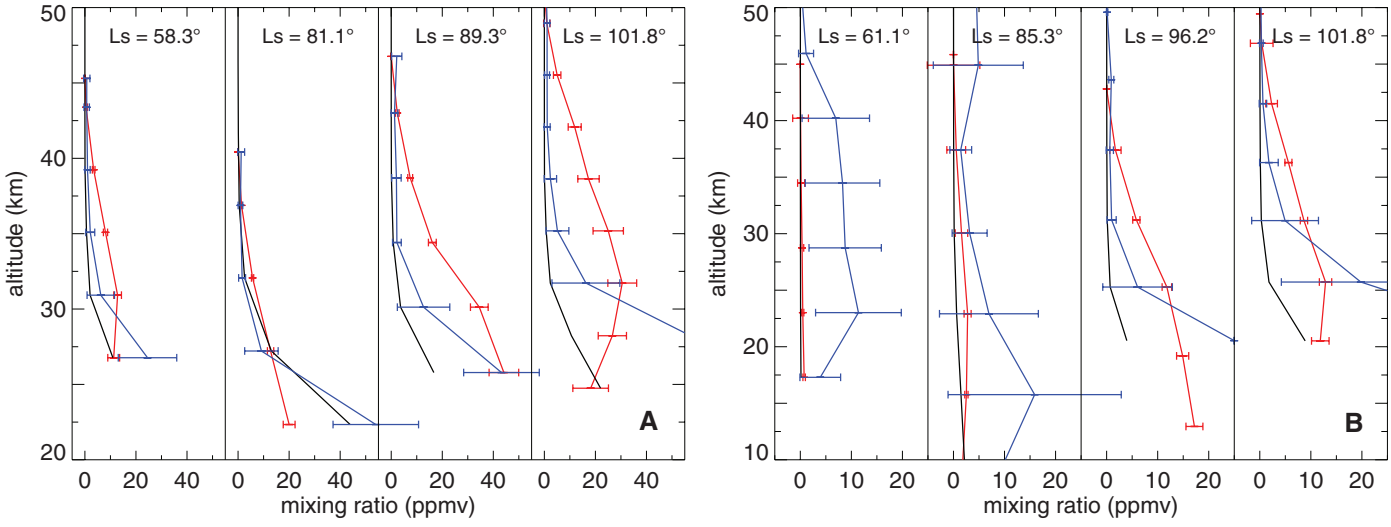

Fig. 2. Selection of typical water vapor volume–mixing ratio profiles in the (**A**) northern and (**B**) southern hemisphere. Black curve, modeled profile by the LMD-GCM; red curve, the retrieved SPICAM results; blue curve, saturation water vapor–mixing ratio. Supersaturation exists where the red values are greater than the blue ones.

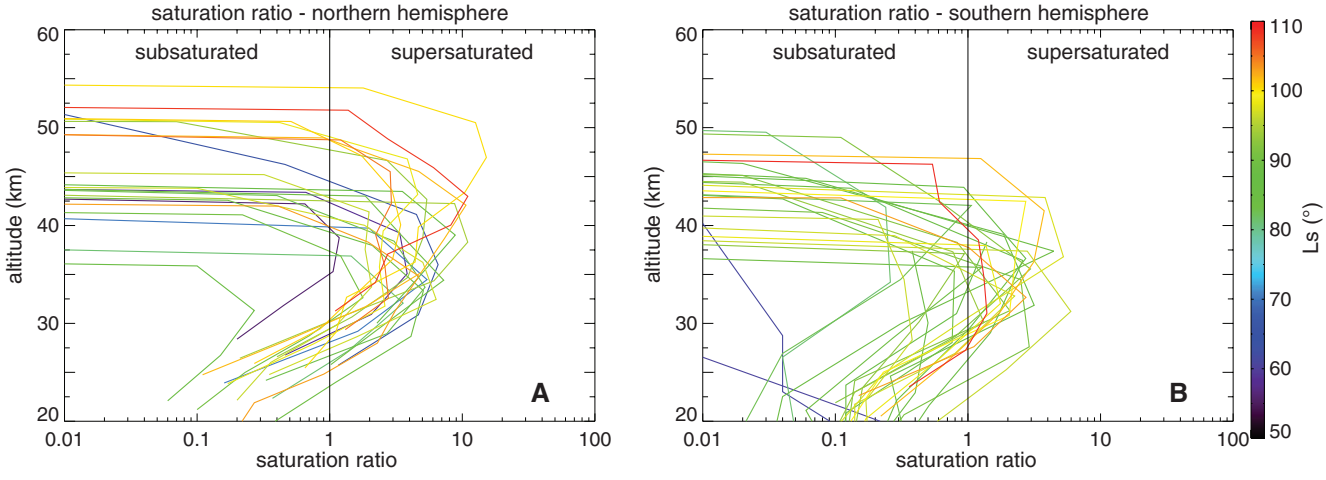

Fig. 3. Saturation ratio for all orbits of the campaign. (**A**) Northern hemisphere. (**B**) Southern hemisphere. The vertical line marks the value of 1, which corresponds to the saturated state.

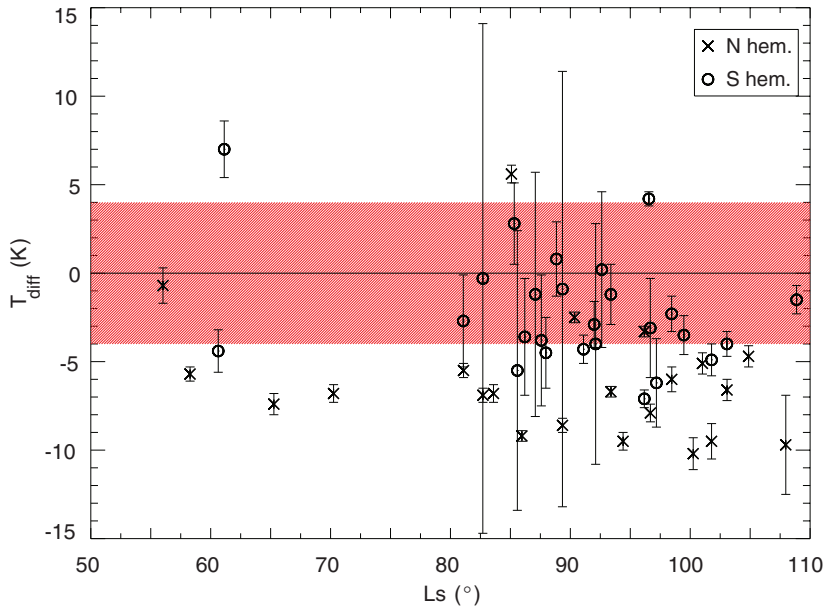

Fig. 4. Temperature difference (T_{diff}) between the actual atmospheric temperature and the condensation temperature for each orbit of the data set, at the altitude where the saturation ratio is biggest, as a function of the solar longitude (L_s). The error bars represent the uncertainties associated with water vapor measurement, and the red region shows the uncertainty on temperature (*16*). Crosses indicate the northern hemisphere orbits, and circles indicate the southern hemisphere orbits. The orbits with no detected water vapor throughout the whole atmosphere are not included.

Supersaturation exists whenever this ratio exceeds 1. Vapor pressure is solely and exponentially dependent on temperature by virtue of the Clausius-Clapeyron equation, making temperature a critical parameter in the definition of the saturation state. We relied on temperature profiles acquired nearly simultaneously by the Mars Climate Sounder (MCS) on the Mars Reconnaissance Orbiter spacecraft in order to correct potential biases in the temperature fields provided by the MCD (*16*, *22*). Our results show that supersaturation is consistently present in the martian atmosphere, at least during the period covered by the observations (Fig. 3). Sixty percent of the data sample exhibits water vapor partial pressures in excess of saturation, and more than 10% shows saturation ratios greater than 5 (table S1). Supersaturation is ubiquitous at northern latitudes, whereas it becomes prominent in the south only after $L_s = 90°$. The values for water vapor supersaturation that we observe on Mars have no counterpart in Earth's troposphere, where saturation ratios rarely exceed 1.5 (*14*). Supersaturation is robust with respect to the uncertainties in temperature estimation and to the retrieval errors, as shown in Fig. 4. The deviation from the condensation temperature is ~5 K on average.

The supersaturation of water vapor on Mars is the likely consequence of a condensation process that becomes inefficient when, for example, there is an insufficient quantity of dust nuclei or when condensation is slowed down by the low-pressure environment of the martian middle atmosphere (*12*, *13*). As occurs with rain on Earth, cloud formations clean the atmosphere locally by capturing condensation nuclei and depositing them in lower layers (scavenging effect). Subsequent excursions of temperature below the freezing point of water will thus not lead to condensation unless new aerosols are supplied locally. In the absence of nuclei, the threshold saturation ratio required to enable the creation of ice crystals exceeds 1000 (*23*, *24*), leaving water vapor free to subsist in a highly supersaturated state. In such a context, an anticorrelation between saturation ratio and atmospheric dust loading is to be expected. This is indeed confirmed in many orbits by simultaneous SPICAM measurements of the aerosol optical depth (*16*). Therefore, the standard assumption of a water vapor profile ultimately controlled by the saturation vapor pressure must be revisited.

The existence of supersaturation has profound consequences for our understanding of the basic mechanisms that have regulated the water cycle on Mars throughout the last billion years. During the northern spring/summer, global atmospheric circulation creates rising motions in the summer tropics. As the air masses are lifted up, they cool adiabatically. This brings their water-holding capacity to the point at which condensation is enabled. This effect is reinforced during the aphelion season because it corresponds to an annual low in insolation and in atmospheric tropical temperature. This mechanism is the basis for the formation of the equatorial cloud belt, one of the most salient and regularly observed features of the climate of Mars (*6*, *11*, *12*). Under the current climatic configuration, the equatorial cloud belt acts like a valve that substantially reduces the cross-hemispheric transport of water during the aphelion season. This atmospheric valve reduces water flow between the hemispheres because cloud formation and the associated scavenging level intersect the upper circulation branch oriented toward the south. This mechanism currently favors the long-term stability and accumulation of water in the northern hemisphere yet favored the southern hemisphere 100,000 years ago, when Mars was in the opposite aphelion phasing. Some of the remnant glaciological features observed at the poles of Mars might be a direct consequence of this valve mechanism (*25*). However, the effectiveness of the aphelion valve depends entirely on how much water in the vapor phase can remain around the hygropause in the tropics and be further advected. Our observations show that as much as 10 to 100 times more water than expected could be present at this altitude, opening the aphelion valve substantially.

Likewise, supersaturation will impact the escape of water from Mars. This process depends on how much water vapor is able to propagate through the hygropause, above which it is photodissociated into the lighter components H and O that will populate the exosphere, where atoms can escape to space. The escape flux of water, which is estimated to form the equivalent of a global layer 5 m thick once integrated over the history of Mars (*26*), is directly proportional to the quantity of water above 20 km, which we argue is much more abundant than previously hypothesized (*27*, *28*). The ramifications of supersaturation extend beyond the sole fate of water; photochemistry will be comparably affected. Considering that water is the precursor of HO_x radicals—the major oxidizing species on Mars—the overall stability of Mars's atmospheric composition is a strong function of the catalytic cycles driven by these radicals (*29*), for which the theoretical production will be substantially altered by our findings of supersaturation in the middle atmosphere (*30*).

References and Notes

1. B. Jakosky, C. Farmer, *J. Geophys. Res.* **87** (B4), 2999 (1982).
2. M. D. Smith, *J. Geophys. Res. Planets* **107**, 25 (2002).
3. L. Maltagliati *et al.*, *Icarus* **213**, 480 (2011).
4. A. Sprague *et al.*, *Icarus* **184**, 372 (2006).
5. M. D. Smith, M. J. Wolff, R. T. Clancy, S. L. Murchie, *J. Geophys. Res.* **114**, E00D03 (2009).
6. R. T. Clancy *et al.*, *Icarus* **122**, 36 (1996).
7. A. Rodin, O. Korablev, V. Moroz, *Icarus* **125**, 212 (1997).
8. D. W. Davies, *J. Geophys. Res.* **84** (B6), 2875 (1979).
9. T. Fouchet *et al.*, *Icarus* **190**, 32 (2007).
10. M. Tschimmel *et al.*, *Icarus* **195**, 557 (2008).
11. M. Richardson, R. Wilson, A. Rodin, *J. Geophys. Res. Planets* **107** (E9), 5064 (2002).
12. F. Montmessin, F. Forget, P. Rannou, M. Cabane, R. Haberle, *J. Geophys. Res. Planets* **109** (E10), E10004 (2004).
13. D. V. Michelangeli, O. B. Toon, R. M. Haberle, J. B. Pollack, *Icarus* **102**, 261 (1993).
14. A. Gettelman, E. J. Fetzer, A. Eldering, F. W. Irion, *J. Clim.* **19**, 6089 (2006).
15. A. Fedorova *et al.*, *Icarus* **200**, 96 (2009).
16. Materials and methods are available as supporting material on *Science* Online.

17. This is according to the martian calendar proposed by (*31*).
18. The solar longitude L_s is the Mars–Sun angle in degrees, measured from the northern hemisphere spring equinox, where $L_s = 0°$. Aphelion occurs at $L_s = 72°$.
19. M. D. Smith, "Mars water vapor climatology from MGS/TES," paper presented at the Mars Water Cycle Workshop, Paris, France, 21 to 23 April 2008.
20. E. Millour *et al.*, *Lunar Planet. Inst. Contrib. Ser.* **1447**, 9029 (2008).
21. Smithsonian meteorological tables (1984), after J. A. Goff, S. Gratch, *Trans. Am. Soc. Heat. Vent. Eng.* **52**, 95 (1946).
22. A. Kleinböhl *et al.*, *J. Geophys. Res.* **114** (E10), E10006 (2009).
23. F. Montmessin, P. Rannou, M. Cabane, *J. Geophys. Res. Planets* **107**, 5037 (2002).
24. A. Määttänen *et al.*, *J. Geophys. Res. Planets* **110** (E2), E02002 (2005).
25. F. Montmessin *et al.*, *J. Geophys. Res. Planets* **112** (E8), E08S17 (2007).
26. H. Lammer, W. Stumptner, S. J. Bauer, *Geophys. Res. Lett.* **23**, 3353 (1996).
27. J.-L. Bertaux, F. Montmessin, *J. Geophys. Res. Planets* **106** (E12), 32,879 (2001).
28. V. Krasnopolsky, *Icarus* **148**, 597 (2000).
29. F. Lefèvre *et al.*, *Nature* **454**, 971 (2008).
30. F. Lefèvre, S. Lebonnois, F. Montmessin, F. Forget, *J. Geophys. Res. Planets* **109** (E7), E07004 (2004).
31. R. T. Clancy *et al.*, *J. Geophys. Res.* **105** (E4), 9553 (2000).

Acknowledgments: We thank L. Montabone for his expertise on MCS data, A. Määttänen for the helpful discussions, and the three anonymous reviewers for their comments that greatly contributed to improve the paper. Mars Express is a space mission of ESA. We thank Centre National d'Études Spatiales (CNES), Centre National de la Recherche Scientifique, and Université Versailles St Quentin en Yvelines in France and Roscosmos in Russia for funding SPICAM. The present analysis was performed with postdoctoral support provided by CNES to L.M. A.F. and O.K. acknowledge Russian Foundation for Basic Research grant 10-02-93116. SPICAM raw data are archived in the Planetary Data System.

Supporting Online Material

www.sciencemag.org/cgi/content/full/333/6051/1868/DC1
Materials and Methods
SOM Text
Figs. S1 to S10
Table S1
References (*32*–*38*)

5 May 2011; accepted 8 August 2011
10.1126/science.1207957

Linking Models of Polymerization and Dynamics to Predict Branched Polymer Structure and Flow

Daniel J. Read,[1] Dietmar Auhl,[2]* Chinmay Das,[2] Jaap den Doelder,[3] Michael Kapnistos,[2] Iakovos Vittorias,[4] Tom C. B. McLeish[5]†

We present a predictive scheme connecting the topological structure of highly branched entangled polymers, with industrial-level complexity, to the emergent viscoelasticity of the polymer melt. The scheme is able to calculate the linear and nonlinear viscoelasticity of a stochastically branched "high-pressure free radical" polymer melt as a function of the chemical kinetics of its formation. The method combines numerical simulation of polymerization with the tube/entanglement physics of polymer dynamics extended to fully nonlinear response. We compare calculations for a series of low-density polyethylenes with experiments on structural and viscoelastic properties. The method provides a window onto the molecular processes responsible for the optimized rheology of these melts, connecting fundamental science to process in complex flow, and opens up the in silico design of new materials.

One of the long-standing fundamental challenges to soft-matter science is the quantitative connection between molecular topology and dynamics of branched entangled polymers. The motivation arises from both the universality of the physics (*1*) and the experimental and engineering properties of highly branched polymers (*2*). Very slow dynamical processes, on time scales of many seconds, emerge even when the entangled macromolecules are of simple linear topology. The additional complication of branching extends the range of relaxation times exponentially and generates additional elasticity in the response to strong extensional flow (*3*). A quantitative account of these phenomena has emerged for very simple polymer structures but has remained elusive in highly complex blends arising from statistical polymerization processes developed in industry (*4*).

The most successful theoretical approach to entangled polymer dynamics is the "tube model" of Doi, Edwards, and de Gennes (*5*, *6*). The model supposes that the topological constraints on any given chain from its neighbors are equivalent to those of a tube around the chain contour. Thus, polymer chains are free to move tangentially along their local contours, but beyond a characteristic "tube diameter," not perpendicular to them. New configurations are always generated by chain ends, as these may explore the surrounding field of chains without constraint. Adding thermal motion to this simple picture immediately predicts qualitatively different dynamics for linear and branched chains. Linear chains diffuse by simple curvilinear diffusion ("reptation") along the tube contour. The orientational configuration of a chosen chain is essentially re-equilibrated by reptation out of its original tube into a new one, a process dominated by a single "reptation time." On the other hand, in branched polymers, reptation is highly suppressed and new configurations of the chains can only be achieved by an exponentially slower "arm retraction" mode (*7*). In this case the chain reconfiguration occurs hierarchically, beginning rapidly at the extremities of entangled arms and ending at segments adjacent to the branch points. These are visited by retracting chain ends only exponentially rarely, thus giving rise to a wide range of experimental relaxation times along the whole entangled arm. Experiments on well-characterized star-polymer melts confirmed such extreme slowing down in both diffusion (*8*, *9*) and rheology (the stress/strain-rate relations that control fluid flow) (*10*). The universal topological nature of the tube theory allows quantitative mapping of its predictions to any particular polymer chemistry and temperature through just two parameters: (i) the "plateau modulus" G_0, which controls the level of elastic stress supported by the melt and which depends on the tube diameter and (ii) the entanglement time τ_e, which sets the time scale of the fastest entangled viscoelastic mode.

Theory and experiment have since been extended to more complex single-molecule topologies: H-shapes (*11*), combs (*12*), and multiarm polymers (*13*, *14*), confirming the predictions of universality over chemistry and the central role of molecular topology. The hierarchical relaxation of entangled star polymers generalizes to more complex architectures: Once free ends retract back to the outermost layer of branch points, these become mobile, activating deeper retractions toward the second layer, and so on (*15*). The relaxation time of a given tube segment in an ensemble of branched polymers depends on the curvilinear distance to the free end that eventually retracts and disentangles it, and on the dangling trees attached to this path that slow down the retraction process (Fig. 1). The prediction of the linear stress-relaxation response of a complex melt therefore reduces to the calculation of the relaxation times by arm retraction of all the segments within it, a program that has been carried through in the case of the simplest cases of polydisperse branched polymers generated by "metallocene" catalysts (*16*).

[1]Department of Applied Mathematics, University of Leeds, Leeds LS2 9JT, UK. [2]Department of Physics and Astronomy, University of Leeds, Leeds LS2 9JT, UK. [3]Dow Benelux B.V., Polyethylene Product Research, P.O. Box 48, 4530 AA, Terneuzen, Netherlands. [4]LyondellBasell Polyolefine GmbH, R&D Polymer Physics and Characterization, Frankfurt, Germany. [5]Departments of Physics and Chemistry, Durham University, Durham DH1 3LE, UK.

*Present address: Bio and Soft Matter (BSMA), Université Catholique de Louvain, Croix du Sud 1, Batiment Boltzmann A201, B-1348 Louvain-la-Neuve, Belgique.
†To whom correspondence should be addressed. E-mail: t.c.b.mcleish@durham.ac.uk